Imaging Simulation for Non-Lambertian Objects Observed Through A Light-Scattering Medium*

Vladimir V. Barun†

Institute of Physics, Belarus Academy of Sciences, The Laboratory of Scattering-Media optics, F. Skaryna Pr. 68, Minsk 220072, Republic of Belarus

Imaging characteristics are covered by the image transfer theory. But up to now, image transfer theory dealt mainly with observation of Lambertian (diffuse reflecting) objects on a Lambertian background. This model of reflection is quite a reasonable one for many natural and artificial objects to describe vision quality. We present here the mathematical description for images of non-Lambertian objects to permit their angular reflection patterns to be dealt with under unfavorable viewing conditions through a light-scattering medium. Retroreflectors are chosen as an convenient example of these objects. The small-angle diffusion approximation of the radiative transfer theory is used for the calculations of light characteristics under illumination by some source of an active vision system. The case studies consider, in particular: (1) Imaging of large-area objects where some of their parts would be seen as dark and others as bright, and (2) the interesting effect of enhancing the contrast of a retroreflector image with increasing optical thickness of a scattering medium. This is related to increasing the "effective" albedo of an "equivalent" Lambertian object, by which the retroreflector can be replaced. The results on imaging characteristics of retroreflective objects are compared with those for Lambertian. The corresponding differences are discussed.

Journal of Imaging Science and Technology 143–151 (1997)

Introduction

May one say with certainty that an object observed is lighter as a whole than its background if the image of the former bears a positive contrast? No, not always. When the angular patterns of object and background reflection are different, the visual perception would depend on the observation direction. Recall a bright Sun's track on a water table to understand that rather a harsh light spot is seen only at the mirror direction. At other viewing angles, smooth water surface will be relatively dark. And what would happen with the contrast of an object image if a layer of a turbid medium is placed between an observer and the object? Usually, the contrast magnitude should decrease. However, the opposite situation shown in this paper can unexpectedly take place too, i.e., the more the shroud, for example, of fog, the better the vision quality. This is also related to features of angular patterns of reflection.

Image transfer through aerosol media is constantly attracting the attention of researchers. Considerable advances in this field have led to the development of modern vision theory.[1] Methods for determining the individual components of radiation power at a receiver have been proposed to characterize image quality. However, all these studies treat, as a rule, observation of diffuse-reflective objects on a Lambertian background, so that already known results cannot be applied directly to a case of another reflection properties.

This paper studies the imaging of non-Lambertian objects. We have selected retroreflectors as these objects for two main reasons. First, their reflective properties differ drastically from that of Lambertian to demonstrate most clearly the distinctive features of observed images. Retroreflectors. the simplest case of which is a well-known corner reflector, feature in that, as their name prompts, they reflect light to the opposite path it is incident on. Secondly, these objects find a wide usage in different scientific and day-to-day fields. For example, retroreflectors are exploited for determining the range from the Earth to space vehicles and communicating with them,[2] measuring light absorption by systems for atmospheric pollution monitoring on the basis of the differential absorption technique,[3] applying retroreflective covers to define overall dimensions of heavy trucks,[4] to make road signs or ad panels, etc.

Problem Formulation and Solution Method

We shall study imaging systems that are often known as active. They comprise a light source, illuminating an object observed through a scattering medium, and a receiver recording a signal. The problem is to find the spatial-angular distribution of signal power P_r at the receiver. Let one observe an object with arbitrary radiance factor $\alpha\left(\vec{R},\vec{n}',\vec{n}\right)$ that depends, in the common case, on spatial $\vec{R}$ and angular $\vec{n},\vec{n}'$ coordinates. Unit vectors $\vec{n}$ and $\vec{n}'$ defined by polar ∂, ∂' and azimuthal φ, φ' angles characterize illumination and reflection directions, respectively. Recall a radiance factor is, by definition, the ratio of light radiance scattered by a medium at point $\vec{R}$ and direction $\vec{n}$ to the radiance reflected by an ideally white Lambertian surface element (with unit albedo) located at the same point and viewed in the same direction under the same Illumination conditions. It can be shown[5] that

$$P_r = \frac{P_o \Sigma_r \Omega_r}{\pi} \int \mu d\vec{n} \int \mu' d\vec{n}' \int I_s\left(\vec{R},\vec{n}\right)\alpha\left(\vec{R},-\vec{n}',\vec{n}\right) I_r\left(\vec{R},\vec{n}'\right) d\vec{R}, \quad (1)$$

where P_o is the light-source power, Σ_r and Ω_r the area and solid angle of the receiver, respectively, $\mu = \cos\partial$, $\mu' = \cos\partial'$,

Original manuscript received December 4, 1995.

* Presented in part at the IS&T/SPIE Symposium on Electronic Imaging: Science and Technology, February 5 - 10, 1995, San Jose, CA, USA, and at The 3rd International Conference on Pattern Recognition and Image Analysis, September 19 - 21, 1995, Minsk, The Republic of Belarus

† Institute of Physics, Belarus' Academy of Sciences, F. Skaryna Pr. 68, Minsk 220072. Belarus. E-mail: ifanbel%basO3.basnet.minsk.by@demos.su

$I_s(\ldots)$ and $I_r(\ldots)$ the radiance distribution over the object surface from the unit-power real and dummy light sources, respectively. The latter is a unit-power too, located as the real receiver and having the same orientation of the optical axis, but with radiation pattern the same as the spatial-angular sensitivity pattern of the real receiver. The notation $\int\ldots d\vec{n}$ abbreviates integration ($\int\ldots d\mu d\varphi$) over angular coordinates, and $\int\ldots d\vec{R}$ over spatial ones. Thus, the problem of object imaging is reduced to the calculation of the radiances $I_s(\ldots)$ and $I_r(\ldots)$ and to the computation of the 6-fold integral according to Eq. 1. Note that Eq. 1 is derived by using only the optical reciprocity theorem,[1] which is valid for the majority of imaging systems and scattering media. No restrictions on system and medium properties are imposed. Therefore, Eq. 1 is of a general character and can be used for any radiation sources and receivers (including an eye) as well as for any media and reflective properties of objects.

Below, we will consider the imaging of objects through a light-scattering medium (e.g., fog) composed of coarse aerosols. Their phase function is known to have a sharp peak in the forward direction. This allows the aspect-invariance principle[1] to be used for the computations. It is valid for small-to-moderate optical thicknesses of a medium, where the "small-angle" approximations of the radiative transfer theory (RTT) are working well. Then, the principle can be shown to result in I_s and I_r dependencies of Eq. 1 on the differences $\vec{R}-\vec{R}_s,\vec{n}-\vec{n}_s$ and $\vec{R}-\vec{R}_r,\vec{n}-\vec{n}_r$, respectively, where $\vec{R}_s,\vec{R}_r$ are the intersection points of the optical axes of the real and dummy sources with the object (or background) surface, $\vec{n}_s,\vec{n}_r$ the directions of their optical axes, i.e.,

$$P_r=\frac{P_o\Sigma_r\Omega_r}{\pi}\int\mu d\vec{n}\int\mu' d\vec{n}'\int I_s\left(\vec{R}-\vec{R}_s,\vec{n}-\vec{n}_s\right)\alpha\left(\vec{R},-\vec{n}',\vec{n}\right)I_r\left(\vec{R}-\vec{R}_r,\vec{n}'-\vec{n}_r\right)d\vec{R}. \tag{2}$$

In particular, for Lambertian objects,

$$\alpha_L\left(\vec{R},\vec{n}',\vec{n}\right)=A_L\left(\vec{R}\right), \tag{3}$$

where $A_L\left(\vec{R}\right)$ is the object albedo. Then, Eq. 2 takes the form

$$P_L=\frac{P_s\Sigma_r\Omega_r}{\pi}\int E_s\left(\vec{R}-\vec{R}_s\right)A_L(\vec{R})E_r\left(\vec{R}-\vec{R}_r\right)d\vec{R}, \tag{4}$$

where $E_s(\ldots)$ and $E_r(\ldots)$ are the irradiances at the object surface produced by the unit-power real and dummy sources, respectively. Eq. 4 is similar to one[6] widely used to describe imaging of Lambertian objects except that the case of $\vec{R}_s=\vec{R}_r$ is considered usually. This case corresponds to a wide radiation pattern of a source, to wide sensitivity pattern of a receiver, or to joint scanning by the said narrow patterns over an object surface, i.e., to situations that often take place for different active vision systems. However, this equality does not hold for illumination by a fixed source with a nonwide radiation pattern (e.g., under illumination by a searchlight or car headlamp) or observation by moving the optical axis of a receiver (e.g., a driver's or other observer's eyes). Then, the more general case described by Eq. 4 should be considered. Note that an active vision system is nonisoplanatic in this case.

For an ideal retroreflector, we have

$$\alpha_{rr}\left(\vec{R},\vec{n}',\vec{n}\right)=\frac{\pi}{\mu}\delta\left(\vec{n}'+\vec{n}\right)A_{rr}\left(\vec{R},\vec{n}\right), \tag{5}$$

where $\delta(\ldots)$ is the delta function. $A_{rr}\left(\vec{R},\vec{n}\right)$ the retroreflector albedo that, in the general case, can depend on spatial and angular coordinates. Substituting Eq. 5 into Eq. 2 gives

$$P_{rr}=P_s\Omega_r\Sigma_r\int\mu d\vec{n}\int I_s\left(\vec{R}-\vec{R}_s,\vec{n}-\vec{n}_s\right)A_{rr}(\vec{R},\vec{n})I_r\left(\vec{R}-\vec{R}_r,\vec{n}-\vec{n}_r\right)d\vec{R}. \tag{6}$$

The forms of Eq. 4 and Eq. 6 are very similar, and their contrast shows the differences in imaging of Lambertian and retroreflective objects through a scattering medium. These differences are discussed elsewhere.[5,7]

Let the irradiances and radiances of Eq. 4 and Eq. 6 be separated into components related to direct superscript d) and scattered (s) light, i.e., represent them in the form

$$I_s=I_s^d+I_s^s,\ E_s=E_s^d+E_s^s, \tag{7}$$

$$I_r=I_r^d+I_r^s,\ E_r=E_r^d+E_r^s. \tag{8}$$

Then, each of the integrals of Eq. 4 and Eq. 6 is partitioned into four integrals comprising combinations of direct and scattered irradiances or radiances produced by real and dummy light sources. At the spatially overlapped real and dummy sources, the integral of the form

$$\int\mu d\vec{n}\int I_s^d A_{rr}I_r^d d\vec{R}$$

for imaging of a retroreflector is expressed via $\delta\left(\vec{n}_s-\vec{n}_r\right)$, i.e., has the singularity at the corresponding point. To avoid dealing with infinities, we will assume below that optical axes of the source and receiver are always separated by some small angle to give $\vec{n}_s\neq\vec{n}_r$, so that the said integral is zero. This singularity is inessential in practice because the angular reflection pattern of a retroreflector always has a finite halfwidth, but Eq. 5 is for an ideal retroreflector. Note that for spatially spaced real and dummy sources of finite dimensions, the above integral is always zero. Below, we will make some additional remarks with respect to allowing for the finite halfwidth.

The components of Eq. 7 and Eq. 8 due to the direct light (with superscript d) attenuate according to the Bougier's law and are easily computed.

As noted above, we will consider the imaging of objects through a fog layer. Let, for simplicity, the optical properties of the medium be independent of spatial coordinates. The phase function of fog is highly forward extended to allow the small-angle diffusion approximation[1] (SADA) of the RTT to be used for computing the scattered components of the light field. The SADA comprises the representation of spatial-angular radiance distributions as the Gaussian functions of the radial $\vec{r}-\vec{r}_s,\vec{r}-\vec{r}_r$ and angular coordinates $\vec{n}_\perp-\vec{n}_{\perp s},\vec{n}_\perp-\vec{n}_{\perp r}$, where $\vec{r},\vec{r}_s,\vec{r}_r$, and $\vec{n}_\perp,\vec{n}_{\perp s},\vec{n}_{\perp r}$ are the projections of $\vec{R},\vec{R}_s,\vec{R}_r$ and $\vec{n},\vec{n}_s,\vec{n}_r$, respectively to the plane of the object viewed (being parallel to the layer boundaries and normal to z axis). Therefore, one has for the case of illumination by a narrow-angle real or dummy source[1]

$$I_{s,r}^s(\tau,\vec{\rho}'_{s,r},\vec{n}'_{\perp s,r})=E_{s,r}^s(\tau,\vec{\rho}'_{s,r})I'_{s,r}(\tau,\vec{\rho}'_{s,r},\vec{n}'_{\perp s,r}), \tag{9a}$$

$$E_{s,r}^s(\tau,\vec{\rho}'_{s,r})=\varepsilon^2S(\tau)S'_{s,r}(\tau,\vec{\rho}'_{s,r}), \tag{9b}$$

$$S'_{s,r}(\tau,\vec{\rho}'_{s,r}) = \frac{1}{2\pi D_{\rho s,r}(\tau)}\exp\left[-\frac{(\rho'_{s,r})^2}{2D_{\rho s,r}(\tau)}\right], \quad (9c)$$

$$I'_{s,r}(\tau,\vec{\rho}'_{s,r},\vec{n}'_{\perp s,r}) = \frac{1}{2\pi D_{\rho\theta s,r}(\tau)}\exp\left\{-\frac{\left[\vec{n}'_{\perp s,r}-\vec{\rho}'_{s,r}A(\tau)/D_\rho(\tau)\right]^2}{2D_{\rho\theta s,r}(\tau)}\right\}, \quad (9d)$$

where $\tau = \varepsilon z$ is the optical thickness of the medium between the source or receiver and object observed (ε is the extinction coefficient and z is the geometrical thickness), $\vec{\rho}'_{s,r} = \varepsilon(\vec{r} - \vec{r}_{s,r})$ the dimensionless radius-vector in the transverse direction (normal to z axis),

$$n'_{\perp s,r} = \left|\vec{\rho}'_{s,r}\right|, \vec{n}'_{\perp s,r} = \left|\vec{n}'_{\perp} - \vec{n}'_{\perp s,r}\right|, S(\tau) = T(\tau)\exp\left[-(1-\Lambda)\tau\right]/\cosh(s\tau),$$

the full radiative flux at optical thickness τ, $T(\tau) = 1 - \exp(-\Lambda\tau)\cosh(s\tau)$, $s = [\Lambda(1-\Lambda)\gamma_2/2]^{1/2}$, Λ the single scattering albedo, γ_2 the second angular moment of the phase function of the medium, $S'_{s,r}(\tau,\vec{\rho}'_{s,r})$ and $I'_{s,r}(\tau,\vec{\rho}'_{s,r},\vec{n}'_{\perp s,r})$ the normalized spatial and spatial-angular distributions of irradiances and radi-ances with variances $D_{\rho s,r}(\tau) = D_\rho(\tau) + D^o_{\rho s,r}(\tau)$ and $D_{\rho\theta s,r}(\tau)$, respectively.

$$D_\rho(\tau) = \frac{1}{1-\Lambda}\left[1 - \frac{\tanh(s\tau)}{s\tau}\right]\frac{1}{T(\tau)}, \quad (10a)$$

where $D^o_{\rho s,r}(\tau)$ depends on the area and angular pattern of the source and, in particular, can be shown by using the aspect-invariance principle[1] to be equal to $\tau^2\beta^2_{s,r}/2$ $\beta_{s,r}$ is the characteristic angular scales of the radiation patterns of the real and dummy sources, respectively) for a point source with Gaussian angular pattern,

$$D_{\rho\theta s,r}(\tau) = D_\theta(\tau) - A^2(\tau)/D_{\rho s,r}(\tau), \quad (10b)$$

$D_\theta(\tau)$ the variance of the angular distribution of an infinitely wide light beam propagating through the medium,

$$D_\theta(\tau) = \frac{1}{1-\Lambda}\frac{\tanh(s\tau)}{T(\tau)}, \quad (10c)$$

$$A(\tau) = \frac{1}{1-\Lambda}\left[1 - \frac{1}{\cosh(s\tau)}\right]\frac{1}{T(\tau)}. \quad (10d)$$

Under illumination by a wide light source, such as the sun, Eqs. 9(a) through 9(d) take the form

$$I^s(\tau,\rho,\vec{n}_\perp) = E^s(\tau,\rho)I'(\tau,\vec{n}_\perp), \quad (11a)$$

$$E^s(\tau,\rho) = E_o S(\tau)S'(\tau,\rho), \quad (11b)$$

$$S'(\tau,\rho) = 1, \quad (11c)$$

$$I'_{s,r}(\tau,\rho,\vec{n}_\perp) = \frac{1}{2\pi D_\theta(\tau)}\exp\left[-\frac{(\vec{n}_\perp)^2}{2D_\theta(\tau)}\right]. \quad (11d)$$

Here E_o is the irradiance from the source at the upper (illuminated) boundaries of the layer and $D_\theta(\tau)$ is determined by Eq. 10c.

As usual for small-angle approximations of the RTT, let light scattered over rather large angles ($\gamma \geq \gamma_o = 45°$) be assumed as absorbed. This assumption is equivalent to introducing an effective medium with single scattering albedo

$$\Lambda = \frac{\Lambda_o}{2}\int^{\gamma_o} p(\gamma)\sin(\gamma)d\gamma, \quad (12)$$

where Λ_o is the true single scattering albedo and $p(\gamma)$ the phase function. For the well-known *Cloud-C1* fog model,[8] $\Lambda = 0.87$ at $\Lambda_o = 1$. Optical parameter γ_2 of the medium can be found[1] from the correlation[8] $\gamma_2 = (1-g)/2$ between γ_2 and the mean cosine g of the scattering angle ($g \simeq 0.86$ for the model in the visible) that gives $\gamma_2 = 0.07$.

We use the representation of the radiance factor of a retroreflector in the form of Eq. 5. Suppose a Gaussian function with halfwidth β_{rr} for its reflection pattern. Values of β_{rr} range[9] within fractions of a degree for retroreflectors of different classes . How will the real halfwidth β_{rr} affect the obtained results? The answer to this question depends on the ratio of β_{rr} to the values $(2D_{\rho\theta})^{1/2}$ for scattered light (terms with superscript s of Eqs. 7 and 8) and to the characteristic scales β_s and β_r of the patterns of the real and dummy sources, respectively, for direct light (superscript d). It can be shown that for $\tau \div 1-3$, where an object can be viewed yet, $(2D_{\rho\theta})^{1/2} \approx 9$ to 12°. Therefore, the angular reflection pattern of a retroreflector can practically be regarded as δ–function in this case to be reasonably expressed in the form of Eq. 5. For the corresponding estimation with respect to direct light from both real and dummy sources, note that we have neglected the term $\int\mu d\vec{n}\int I^d_s A_{rr} I^d_r d\vec{R}$. For finite β_{rr} and coincident real and dummy sourses,

$$\int\mu' d\vec{n}'\int\mu d\vec{n}\int I^d_s \exp[-(\vec{n}-\vec{n}')^2/\beta^2_{rr}]I^d_r d\vec{R} \sim= \exp(-2\tau)\exp[-(\vec{n}_r - \vec{n}_s)^2/\beta^2_{rr}],$$

i.e., is rather small at the corresponding values of τ and $(\vec{n}_r - \vec{n}_s)^2/\beta^2_{rr}$. In the following, we will continue to neglect this term, that is we neglect the sharp narrow peak [having the value proportional to $\exp(-2\tau)$] near direction $\vec{n}_r = \vec{n}_s$.

Sample Results

We consider below some examples to illustrate several cases where visual perception and image characteristics of retroreflectors are radically different from that of Lambertian objects under observation through a light-scattering medium such as fog. Using the methodology of the previous section, object images are derived analytically by quite a simple way. Really, one would derive the desired formulas describing the imaging by substituting Eqs. 9 through 11 into Eqs. 4 and 6 and performing the integration to obtain the results in the final analytical form. The calculations were made under the assumption that the light receiver is a human eye to provide its representation as a dummy point source with the divergence of some arc minutes. This allows us to treat the radiation pattern of the dummy source, corresponding to an eye, as δ-function of both spatial and angular coordinates. For simplicity, the albedos of retroreflective and Lambertian objects will be assumed to have constant values dependent on neither spatial nor angular coordinates.

Visual Perception of Retroreflective Objects having Different Dimensions. Visual perception of an object is determined, mainly, by a light signal arriving at an eye, further processing of the signal by the human brain, and accompanying physico-chemical processes. We consider here only the optical problem for an approach to the solution to the first stage of this complex sequence. The case of observation of a retroreflective or Lambertian object against a Lambertian background is taken as the basis for quantitative estimations and qualitative illustrations. A square with side $2b$ is the object. Two types of illumination are considered, i.e., by light sources with wide (Figs. 1 through 3) and rather narrow (Fig. 4) radiation patterns. The first can be used as a model of illumination by, e.g., street lights or antifog headlights along the horizontal axis (to do so[10] one needs to invoke the aspect-invariance principle[1] too) whereas the second one can serve to simulate the illumination by high or low beam of a car, etc.

Below, the object size will be expressed in the units of the characteristic size of light-ray radial spreading in a scattering medium, i.e., in the units of $d = (2D_r)^{1/2}$, where $D_r = D_\rho/\varepsilon^2$ is the dimensional variance of the SADA to be computed by Eq. 10a. Fig. 1 shows the signal profiles that arrive at an eye from the object and background common plane under illumination and observation through a fog layer with optical thickness $\tau = 1$ [top line, cases 1(a) through 1(c)], $\tau = 2$ [middle, 1(d) through 1(f)], and $\tau = 3$ [bottom, 1(g) through 1(i)]; i.e., Fig. 1 illustrates only a so-called object component without taking backscattering interference into account. The illumination is along the normal to the object plane. Here, the values of $P = P_{rr}/\Omega_r \Sigma_r E_o$ (solid lines) or $P_L/\Omega_r \Sigma_r E_o$ (dashed lines), where E_o is the irradiance produced by the source at $z = 0$, are computed via Eqs. 11a through 11d. The left [1(a), 1(d), and 1(g)], middle [1(b), 1(e), and 1(h)], and right [1(c), 1(f), and 1(i)] columns of Fig. 1 correspond to the decreasing object size $b = 3d$, d, and $0.1d$ respectively. The image is formed by scanning the eye along the mean line of the square (along the x-coordinate). (An eye is a multielement receiver of optical radiation, and such scanning often includes the recording of radiation by its different elements.) Point $X = 0$, $Y = 0$ corresponds to the center of the square, and X-, Y-values are measured in b-units. i.e., $X = x_r/b$, $Y = y_r/b$, where x_r, y_r are the dimensioned coordinates of the intersection point of the receiver's optical axis with the object plane ($\vec{r}_r = \{x_r, y_r\}$). Thus, the object occupies the space $|X|$, $|Y| \leq 1$, and background $-|X| > 1$ at any Y or $|Y| > 1$ at any X. Here, the location of the receiver has coordinates ($x_r = 0$, $y_r = 0$, $z_r = 0$), the object albedo $A_o(A_{rr}$ or $A_L) = 0.3$ and that of background $A_b = 1$.

Consider first Figs. 1(a), 1(d) and 1(g). The appearance of a large (with respect to d) uniform retroreflective object (solid lines) changes considerably. For $\tau = 1$ or 2, an observer would see a clear small spot near the center of the object. Note that this spot is brighter than the background even though $A_o < A_b$. With increasing τ, the spot becomes darker than the background [see Fig. 1(g)], but is clearer than surrounding regions of the retroreflector. At the peripheral parts of the square, dark belts along four sides of the real object are detected. The outer borders of these belts coincide with the real boundaries of the square. We will not give a quantitative estimation of the border locations of these regions here, but will restrict ourselves by a qualitative description to attract one's attention to the image transformations. So, the observer could think, e.g., that he sees two objects with variable brightness instead of the single original square illuminated by a uniform wide light beam with constant albedo, or that reflective characteristics change substantially along the object surface. Note that the similar Lambertian object appears in the usual way being approximately uniformly dark against a clear background.

At smaller object sizes [Figs. 1(b), 1(e) and 1(h)], the retroreflector images are featured not only by inverted brightness as contrasted with that of the images of the Lambertian object, but because of the influence of a scattering medium, give wrong information on the object shape and dimensions too. Indeed, the retroreflective square looks essentially like a clear circle (note once more that $A_o < A_b$) having a diameter larger than the side of the original object. Image brightness is again variable, being maximal near the true center of the object to decrease monotonically toward the edges.

Only for small objects [Figs. 1(c), 1(f) and 1(i)], would an observer see the real contours of a retroreflective object, but its Lambertian background with $A_b = 1$ would look dark. So, one could say as if the albedo of a retroreflector has increased to introduce the "effective' albedo of a Lambertian object, the retroreflector could be replaced by. This question will be considered in the next subsection.

Figure 2 shows the object component profiles along the x-coordinate for the same large-area retroreflective square ($b = 3d$) and $\tau = 2$ at different Y values. Figure 2(a) is the same as Fig. 1(d) ($Y = 0$). One would see the transformations of the central spot of the images with increasing Y and approach of these profiles to that of the Lambertian object [cf. solid and dashed curves in Fig. 2(d)].

Simulated 2D images (only object components) of the retroreflective squares with halfside $3d$, d, and $0.1d$ observed through the model fog layer having $\tau = 2$ are illustrated in Figs. 3(a), 3(b), and 3(c), respectively. These images represent vividly all the above features. Note the images of Fig. 3 are normalized by some other way in contrast with that of Fig. 1 through Fig. 2; i.e., their brightness values are equalized in the center of the square.

A more intricate situation takes place under illumination of a retroreflective object by a source with a narrow radiation pattern (Fig. 4). The source is assumed as point one providing a divergent light beam with characteristic angle $\beta_s = 10°$. Here are illustrated the images of objects with albedo only 0.02 observed on Lambertian background with $A_b = 1$ for the source and receiver located at the same point. As in Fig. 1, the top, middle, and bottom lines of Fig. 4 give object component profiles for $\tau = 1$, 2, and 3, respectively. The left column of Fig. 2 corresponds to the case when the center of the light spot and that of the object coincide, but the right one corresponds to the case when there is a distance of $0.2b$ between the said centers along x-axis. Object size $b = d$ here. Signal power values are normalized by $P = P_{rr}/\Omega_r \Sigma_r \varepsilon^2$ (solid lines) or $P_L/\Omega_r \Sigma_r \varepsilon^2$ (dashed). All the features mentioned with respect to Fig. 1 are also observed here. However, the pictures are more complicated because of the superimposition of the above effects of Fig. 1 on nonuniform illumination. We will not give a detailed description of the resulting images, but note only that the amplification of real albedo of a retroreflector is more pronounced under illumination by such a source. Really, a retroreflector can be seen as a clear object under such a large difference in the albedos.

Effective Albedo of a Retroreflector. Figures 1 and 4 show a retroreflective object as having a higher effective albedo than the real one. The reason for such an increase is rather obvious: radiation is reflected strictly backward, being directed preferably to the receiver. The analytical expression for the effective albedo is derived quite simply. By substituting the explicit form of I_s and I_r according to the SADA into Eq. 6 and integrating, one obtains that, at a small-sized retroreflector [$b << (2D_r)^{1/2}$,

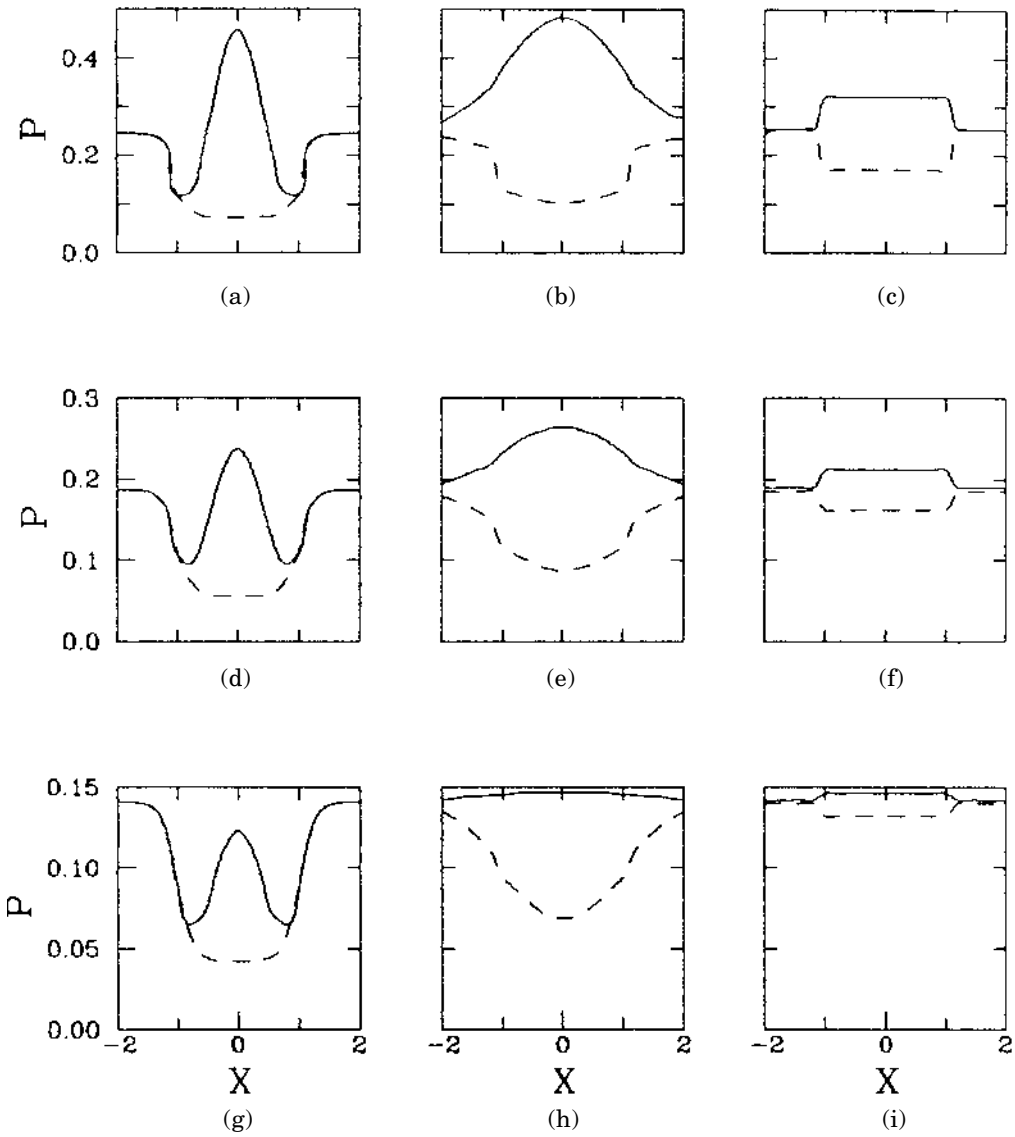

Figure 1. Signal power profiles from retroreflective (solid lines) and Lambertian (dashed lines) objects observed through the model scattering medium *Cloud C-1* with optical thickness (a) through (c), $\tau = 1$; (d) through (f), $\tau = 2$; (g) through (i) $t = 3$, under illumination by a wide light beam for $Y = 0$ and $A_o = 0.3$, $A_b = 1$. Object—square with side $2b$, $b = 3d$ (left column), d (middle column), and $0.1d$, (right column).

here b is not necessarily the side of a square, but a characteristic size of an object], a retroreflective object with albedo A_{rr} can be approximately replaced by a Lambertian one having effective albedo $\alpha(\tau)A_{rr}$. For $(s\tau)^2 << 1$ and illumination by a wide light beam,

$$\alpha_d^w(\tau) = \frac{1}{8D_{\rho\theta}(\tau)} \exp\left[-\frac{\delta^2}{8D_{\rho\theta}(\tau)}\right], \tag{13}$$

under imaging preferably by direct light (here, δ is the angle between the optical axes of a source and receiver), i. e., under the main contribution to P_{rr} (see Eq. 6) from the integrals of the type $\int \mu d\vec{n}' \int I_s^d A_{rr} I_r^s d\vec{R}$ or $\int \mu d\vec{n}' \int I_s^s A_{rr} I_r^d d\vec{R}$; and

$$\alpha_s^w(\tau) = \frac{1}{10D_{\rho\theta}(\tau)} \exp\left[-\frac{\delta^2}{16D_{\rho\theta}(\tau)}\right], \tag{14}$$

under the dominant contribution of scattered light to an image, i.e., under the main contribution to Eq. 6 from $\int \mu d\vec{n}' \int I_s^s A_{rr} I_r^s d\vec{R}$, where $D_{\rho\theta}(\tau)$ is determined by Eq. 10(b). When a retroreflector image is formed by both direct and scattered light, that is for contributions from the above integral types being the same order, α takes some intermediate value relative to that given by Eqs. 13 and 14 respectively. Similar formulas can be derived[11] for illumination by a narrow-angle light beam. Note that the condition $(s\tau)^2 << 1$ is valid practically at all the values of τ when an object still can be seen.

As follows from Fig. 1 through 4, effective albedo of a large-sized retroreflector would depend on the coordinates of a point within its area and vary over the object surface. Hence, the introduction of the effective albedo is not so useful here. Nevertheless, one could do this in an analytical form by substituting the explicit expressions for I_s and I_r of Eqs. 9, and 10 into Eq. 6 to replace a retroreflector by a Lambertian object with the said albedo value.

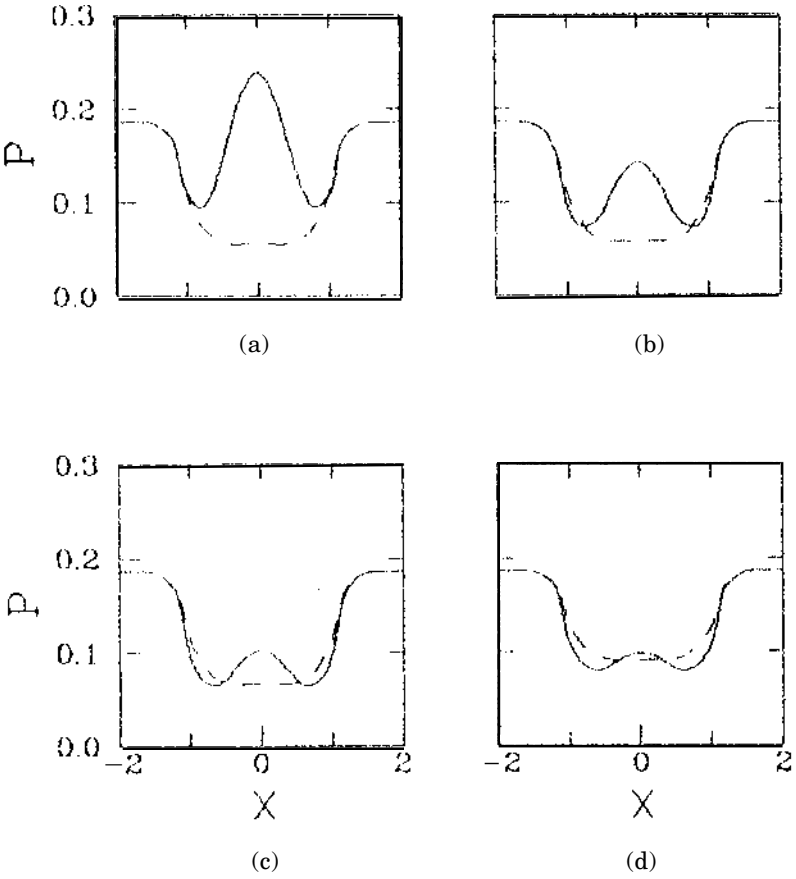

Figure 2. Signal power profiles from retroreflective (solid lines) and Lambertian (dashed lines) objects observed through the model scattering medium *Cloud C-1* with optical thickness $\tau = 2$ under illumination by wide light beam for (a) $Y = 0$, (b) $0.5d$, (c) $0.7b$, and (d) $0.9b$, $A_o = 0.3$, $A_b = 1$. Object—square with side $2d$.

Unusual Behavior of the Contrast of Retroreflector Image. By definition, the contrast κ of an object image is $\kappa = P_{vs}/P_{\text{int}}$, where P_{vs} and P_{int} are the power values of valid signal and optical interferences, respectively. The valid signal is understood as the difference of signals corresponding to two points of an image; one of these points belongs to the object image and the other to the background. Optical interferences comprise the sum of signal power from the background against which the object is viewed and power of backscattering interference because of a medium between the object and receiver. Above, we have studied the object components of the signals (P values at $|X|, |Y| \le 1$ and $|X| > 1$ or $|Y| > 1$, respectively in Fig. 1 through Fig. 3). To compute the backscattering interference power, we have used the method[12] described in Ref. 5 as applied to the problem considered here. The description of this method will not be included in this paper.

Because of increasing effective albedo of a retroreflector, a question arises on changes of its contrast with optical thickness. Really, as seen from Eqs. 13 and 14, the albedo gain $\alpha(\tau)$ has a maximum as a function of τ. So, two competing processes would take place at growing τ to affect κ in opposite directions. The first is the increase in $\alpha(\tau)$ up to the maximum, thus enhancing the contrast. The second consists of the attenuation of the valid signal and growth of the backscattering interference to lead to the contrast decrease. The combined action of these two processes results in the dependences of the contrast magnitude of retroreflector images shown in Fig. 5. This illustrates the case of illumination of a small retroreflector by a wide light beam and its observation against a Lambertian background with albedo $A_b = 0.4$. Object albedo ranges from 0.1 (curve 1) to 0.2 (curve 3). At low τ, contrast magnitude $|\kappa|$ decreases, contrast itself being negative and the object darker than the background. Then, at intermediate τ, the object becomes invisible because its image has negligible contrast, and during further submerging into a scattering medium, it appears as clear (although $A_o < A_b$). And what is most interesting is a maximum of the contrast at some optical thickness. In other words, there is an optimal τ value where a retroreflector would be viewed most clearly, other conditions being fixed.

Conclusion

This paper has presented an approach to treating imaging, in general, and visual perception in its first stage, in particular, of objects with arbitrary reflection diagrams. We considered here the observation of retroreflective objects through a light scattering medium. Their images formed by an active vision system show a number of surprises. First, a retroreflector may be visually perceived as two different objects. An image of a retroreflector being illuminated uniformly and having constant reflective characteristics can be highly nonuniform in brightness, etc. Second, a retroreflector with very low albedo located against the ideally white Lambertian background may be viewed as a clearer object than the background. We give a quantitative estimation of the albedo gain. This effect of albedo amplification by a scattering medium leads to interesting unusual behavior of the contrast of a retroreflector image. The dependence of the contrast on optical thickness of a medium can have a maximum to provide the best conditions of object observations for a case when a retroreflector is submerged into the medium rather than "lying on its surface." This mechanism of contrast enhancement can be set up as a hypothesis for improving visibility of objects from space

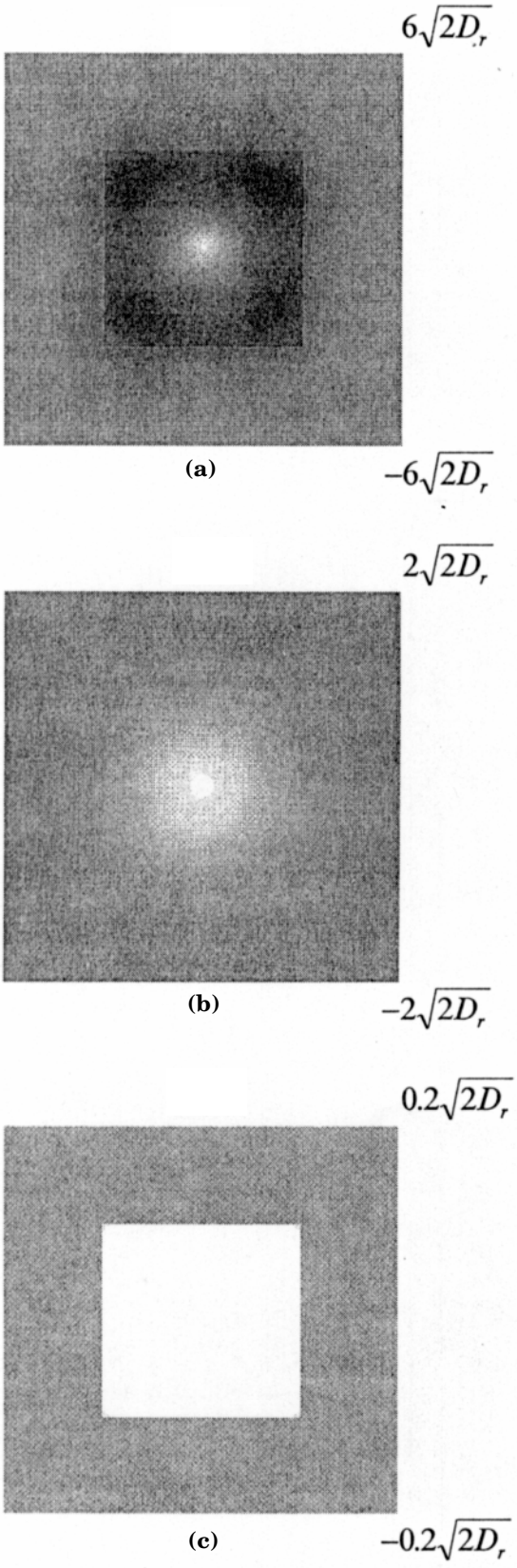

Figure 3. Simulated 2D images (only object components) of the retroreflective squares with halfside (a) $b = 3d$, (b) d, and (c) $0.1d$ observed through the model scattering medium *Cloud C-1* of optical thickness $\tau = 2$ under illumination by wide light beam.

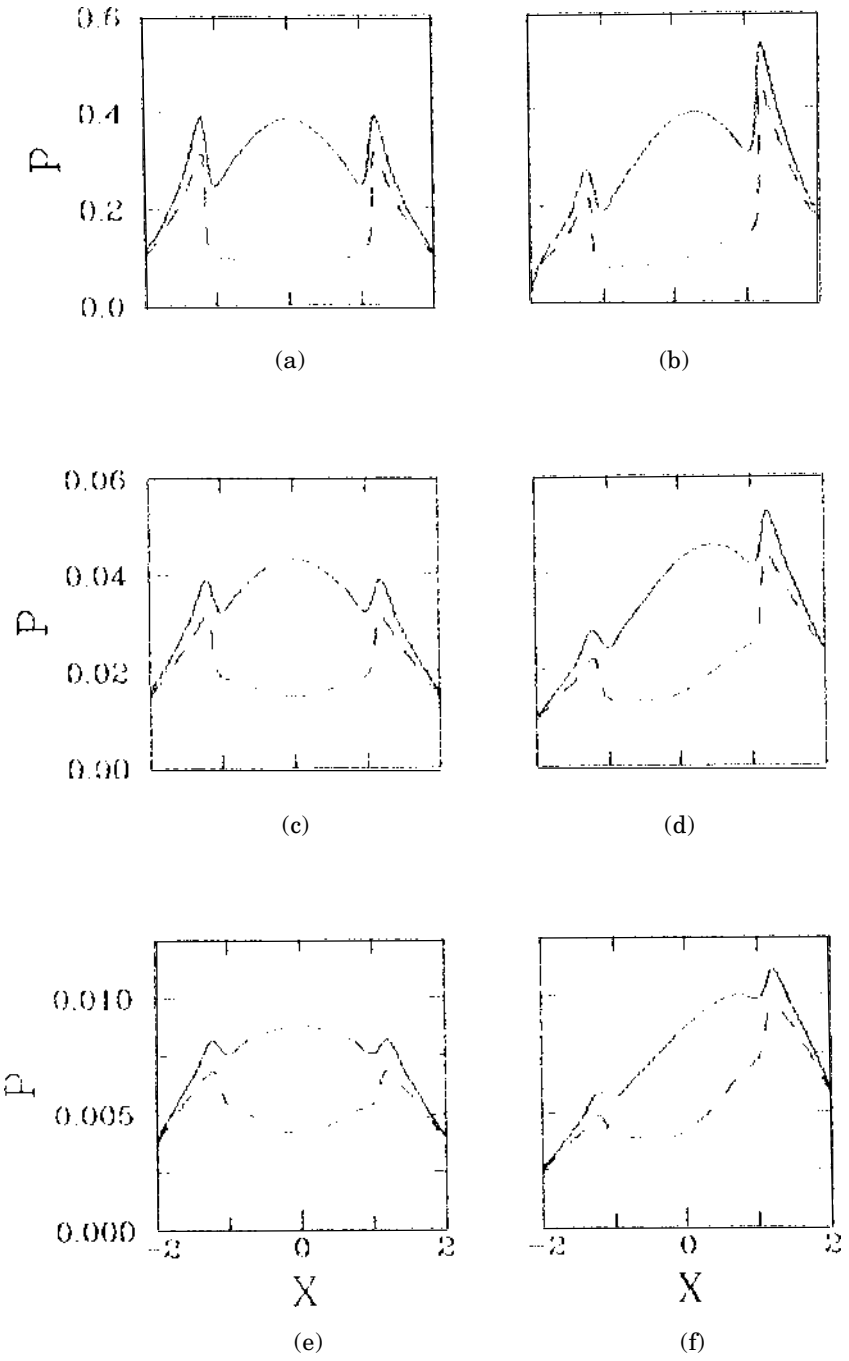

Figure 4. Signal power profiles from retroreflective (solid lines) and Lambertian (dashed lines) objects observed through the model scattering medium *Cloud C-1* with optical thickness (a) and (b) $\tau = 1$, (c) and (d) $\tau = 2$ and (e) and (f) $\tau = 3$ under illumination by narrow-angle ($\beta_s = 10°$) light source for $Y = 0$ and $A_o = 0.02$, $A_b = 1$. Object—square with side $2d$. The center of the light spot coincides with the center of the object (left column) and is $0.2d$-spaced from it (right column).

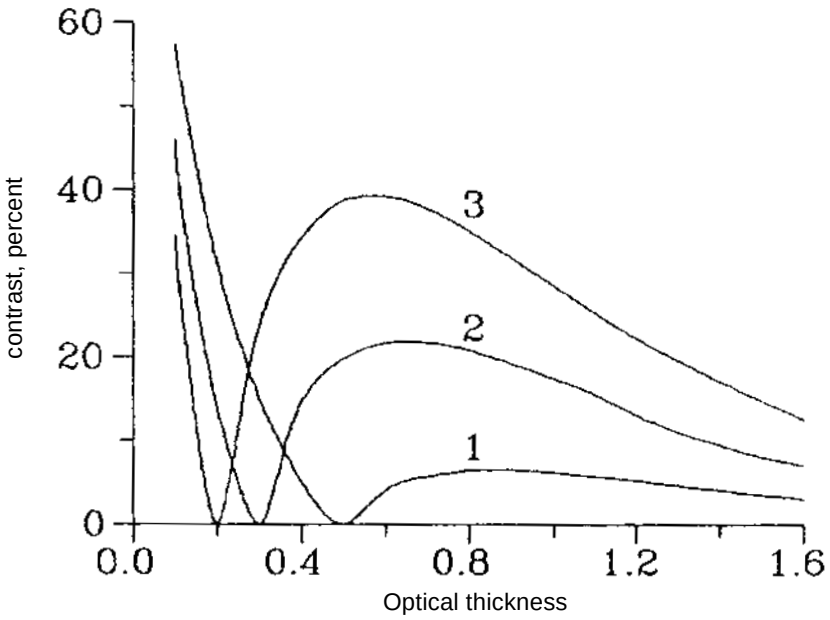

Figure 5. Image contrast for a small retroreflector illuminated by wide light beam as a function of optical thickness of the model scattering medium Cloud C-1 for A_{rr} = 0.1 (curve 1), 0.15 (curve 2), 0.2 (curve 3), A_b = 0.4.

as compared with that from low altitudes, i.e., as a hypothesis explaining the fact being repeatedly told us by astronauts. However, the hypothesis requires further investigations to substantiate.

Acknowledgments. The author would like to thank the International Scientific Foundation (Soros' Foundation) for the financial support and travel grant to present this Paper at IS&T/SPIE's Symposium on Electronic Imaging: Science and Technology, February 5–10, 1995, San Jose, CA. The assistance of Mr. A. S. Prikhach, a research scientist from the Institute of Physics, Minsk, Belarus, in computer graphics is also highly appreciated.

References

1. E. P. Zege, A. P. Ivanov, and I. L. Katsev, *Image Transfer through a Scattering Medium,* Springer-Verlag, Heidelberg, 1991. Chaps. 4 and 5.
2. P. A. Lightsey, Scintillation in ground-to-space and retroreflected laser beams, *Opt. Eng.* **33:** 2535 (1994).
3. H. Edner, P. Rasnarson S. Spahnare, and S. Svanberg, Differential optical absorption spectroscopy (DOAS) system for urban pollution monitoring, *Appl. Opt.* **32:** 327 (1993).
4. V. F. Koutenev and B. V. Kisoulenko, Russia as a member of Geneva 1958's Agreement on auto- and motorvehicles, *Proc. NAMI*: **3** (1993). in Russian.
5. V. V. Barun, Imaging of retroreflective objects under highly nonuniform illumination, *Opt. Eng.,* **35**: 1894 (1996).
6. D. M. Bravo-Zhivotovsky, L. S. Dolin, A. G. Luchinin, and V. A. Saveljev, Some questions of vision theory through turbid media, *Izv. AN SSSR, Sov. Fiz. Atmos. Ocean* **5:** 672 (1969), in Russian.
7. V. V. Barun, Visual perception of retroreflective objects through light--scattering media, *Proc. SPIE* **2410:** 470 (1995).
8. D. Deirmendjian, *Electromagnetic Scattering on Spherical Polydispersions*, Elsevier, New York, 1969, Chap. 3.
9. *Visual aspects of road markings, Joint Technical Report CIE/PIARC*, 1986, 121 p.
10. V. V. Barun, Rain, dust, and snow effects on anti-fog headlight performance, *Proc. SPIE* **2222:** 276 (1994).
11. V. V. Barun, Peculiarities in observation of retroreflective objects through a scattering medium, *Izv. RAN, Sov. Fiz. Atmos. Ocean,* **33**: 62 (1997) in Russian.
12. E. P. Zege, I. L. Katsev and I. N. Polonsky, Analytical solution of radar equation for cloud sounding taking into account multiple scattering, in *Proc. XV Int. Laser Radar Conf. IOA SO AN USSR,* Tomsk, 1990, 333–337.